Indian Journal of Pure & Applied Physics
Vol. 64, October 2026, pp. 1148-1153
DOI: 10.56042/ijpap.v64i10.33155

Comprehensive Structural and Vibrational Insights into Electron Beam Deposited Copper Thin Films

Minakshi[a*], Kirti Nanda[b], Dimple Balan[c], Rita Rani[a] & Devendra Mohan[d]

[a]Department of Physics, Ch Mani Ram Godara Government College for Women, Fatehabad 125 050, India
[b]Department of Physics, Guru Gorakhnath Ji Government College, Hisar 125 004, India
[c]Department of Physics, Guru Jambheshwar University of Science & Technology, Hisar 125 001, India
[d]Department of Applied Science, Panipat Institute of Engineering and Technology, Samalkha, Haryana 132 102, India

Received: 28th June 2026; accepted: 6th August 2026

A cost-effective Electron beam evaporation technique with post-oxidation was used to deposit copper oxide thin films.The microstructural analysis was done by Rietveld refinement using Fullprof software. Rietveld refinement showed that prepared films had monoclinic structure with space group C2/c. From Rietveld analysis lattice parameters and Interplanar spacing was calculated for all the prepared samples. Raman spectroscopy confirmed the successful transformation of metallic copper to copper oxide phase.XPS analysis confirmed the presence of Cu^{2+} oxidation states demonstrating the successful formation of CuO. The combined structural and chemical analysis demonstrates that the prepared films possess improved phase purity making them suitable for applications in optoelectronics, sensing, and nonlinear optical devices.

Keywords: Electron beam evaporation, Oxidation, Rietveld refinement, Raman spectroscopy, X-ray spectroscopy

1 Introduction

Over the past several years, nano range semiconductors have emerged as a compelling counterpart to traditional bulk semiconductors. Their appeal lies not only in the profound size dependent modifications of their physical properties an aspect that continues to challenge and enrich fundamental research but also in their wide ranging technological potential. These materials are now central to advances in nano-electronics, photonics, opto-electronics, biomedical nanotechnology, and the development of renewable energy nano-devices, underscoring their transformative role across multiple scientific and engineering domains. In today's era transition metal oxides have reached a vital place in several fields of chemistry, physics and material science. Currently copper oxides specially found a broad application domain in catalytic field emission, gas sensing, lithium batteries and solar cells.

Copper oxide (CuO) has a monoclinic crystal structure with variable optical energy band gap typically ranging between 1.3 and 2.1eV, making it highly versatile for numerous applications. These low bandgap semiconductors are very useful in photo-thermal and photoconductive applications[1]. This is p-type semiconductor, due to unique properties; this material finds extensive application in photovoltaic systems, gas detection sensors, magnetic storage devices, and catalytic processes. CuO, along with Cu_2O, represent the stable copper oxide phases under normal conditions. However, there are also a number of meta-stable copper oxide phases like Cu_2O_3, Cu_3O_2, and Cu_4O_3, which introduce additional structural diversity and range of properties[2-7]. The crystal structure of copper oxides are cubic, monoclinic, and tetragonal forms which contribute to a broad spectrum of electrical and optical behaviors depending upon the synthesis condition. Copper oxide thin films tend to exhibit a mixture of phases, specifically Cuprous oxide and Cupric oxide, when oxidized or annealed at relatively low temperatures around 350°C, as reported in the literature[8].The wide range of properties of copper oxide has drawn considerable interest, with researchers employing various synthesis techniques such as Chemical Vapour Deposition (CVD), vacuum evaporation, sol-gel processing and sputtering to create CuO films[9-10]. It has diverse applications across several advanced technologies. They are used in photo-electrochemical cells, batteries, and gas sensors, as well as in energy

*Corresponding author: E-mail:minakshimakkar90@gmail.com

harvesting and storage. It also serves as effective photo-catalysts, are utilized in field-emission devices, superconductors, and play a crucial role in photovoltaic devices for solar energy conversion[11-19]. Due to its non-toxic nature, it holds great potential for use in biomedical and biological applications[20-21].

The thermal thermodynamic budget plays a vital role in governing the phase purity, nucleation kinematics, and structural evolution of the copper oxide thin films. To evaluate this effect, the films were systematically investigated at three distinct annealing temperatures: 400°C, 500°C, and 600°C. Preliminary characterisation trials conducted below this window at 300°C resulted in an incomplete chemical reaction, yielding an undesirable mixed-phase matrix due to insufficient thermal activation energy.

Consequently, 400°C represents the critical threshold where complete phase stabilization is achieved, showing a highly pure, single-phase crystalline matrix free from secondary structural impurities. As the annealing temperature is further elevated to 500°C, a marked improvement in structural crystallinity is observed, characterized by sharper Bragg reflections and a substantial reduction in the full-width at half-maximum (FWHM) due to thermally driven grain coalescence. However, further increasing the thermal processing to 600°C induces excessive lattice strains and potential micro-structural cracking caused by substrate thermal mismatches. Therefore, 400°C is identified as the optimum phase-growth nucleation temperature required to successfully eliminate mixed-phase contamination, while 500°C serves as the optimum regime for maximizing structural grain development without compromising the physical stability of the matrix."

In the present study, copper thin films were prepared using easy and high quality thin films fabrication method which is Electron beam evaporation technique and prepared films were annealed at temperature 400 °C, 500 °C and 600 °C for duration of 5 hours named as S1,S2 and S3 samples respectively. The thermal treatment plays an important role in phase purity, nucleation kinematics, and structural evolution. To evaluate this effect, the films were systematically investigated at three distinct annealing temperatures: 400°C, 500°C, and 600°C. Preliminary characterisation trials conducted below this window at 300°C resulted in an incomplete chemical reaction, yielding an undesirable mixed-phase matrix due to insufficient thermal activation energy. Consequently, 400°C represents the critical threshold where complete phase stabilization is achieved, showing a highly pure, single-phase crystalline matrix free from secondary structural impurities. As the annealing temperature is further elevated to 500°C, a marked improvement in structural crystallinity is observed, characterized by sharper Bragg reflections and a substantial reduction in the full-width at half-maximum (FWHM) due to thermally driven grain coalescence. However, further increasing the thermal processing to 600°C induces excessive lattice strains and potential micro-structural cracking caused by substrate thermal mismatches. Therefore, 400°C is identified as the optimum phase-growth nucleation temperature required to successfully eliminate mixed-phase contamination, while 500°C serves as the optimum regime for maximizing structural grain development without compromising the physical stability of the matrix.For detailed analysis of microstructural parameter like lattice parameter and volume of unit cell Rietveld Refinement method was used. For confirmation of phase purity chemical analysis was done using Raman and X-ray Photo-spectroscopy. Integrated structural and compositional analyses confirm that the fabricated films exhibit enhanced single phase purity, thereby rendering them highly suitable for deployment in optoelectronic systems, sensing platforms, and nonlinear optical devices.

2 Materials and Methods

Copper thin films were synthesized using the E-beam Evaporation technique under a high vacuum environment. Prior to deposition, the glass substrates underwent a rigorous chemical cleaning protocol involving sequential ultrasonic sonication in acetone, ethanol, and deionized water, followed by drying under a high-purity nitrogen stream. The target material (Cu source) was loaded into a water-cooled copper crucible, while the cleaned substrates were mounted on a rotating substrate holder positioned directly above the evaporation source to ensure thickness uniformity. The deposition chamber was subsequently evacuated to a base pressure of approximately 10^{-5} to 10^{-6}Torr using a combination of rotary and diffusion vacuum pumps. Once the desired base vacuum was achieved, a thermionically emitted electron beam from a tungsten filament was accelerated via a high-voltage power supply and magnetically deflected onto the Copper target. The intense kinetic energy of the focused electron beam rapidly melted and vaporized the target material, generating a vaporcloud that condensed onto the

cooler surface of the substrates. The deposition rate and the final film thickness (~740nm) were precisely monitored in real-time using a calibrated Quartz Crystal Microbalance (QCM) sensor system. After the deposition of metal films (copper), the films were placed in muffle furnance for oxidation at temperature 400 °C, 500 °C and 600 °C.

2.1 Characterization Techniques

Rietveld refinement was done using Fullprof suite software using XRD data. Raman spectroscopy was performed using a Witec UHTS 300 SMFC Green-NIR system, employing a 532 nm green laser as the excitation source, to classify the phases of copper oxide in the oxidized films. XPS was performed using ICP-MS, CHNSO analyzer.

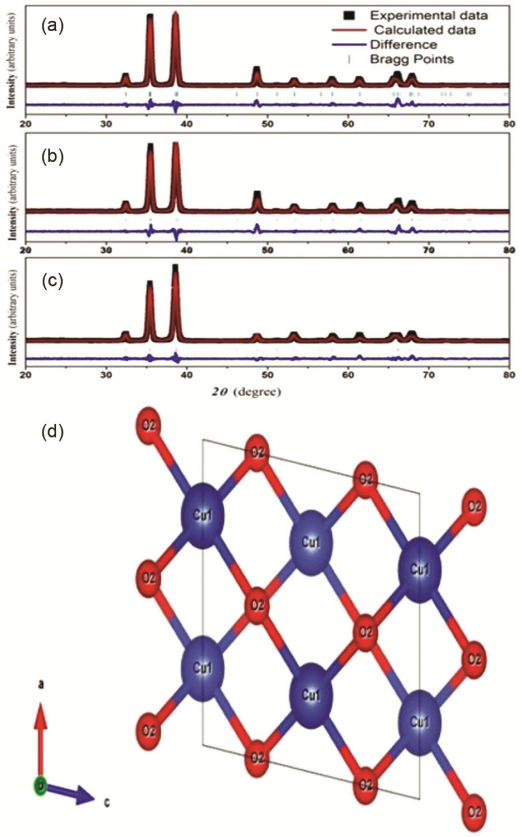


Fig.1 — Refined XRD pattern of CuO thin films oxidized at (a) 400°C (b) 500°C (c) 600°C; and (d) Crystal structure of copper oxide from refinement data using VESTA software

3 Results and Discussion

3.1 Microstructural Parameters using Rietveld Refinement

To thoroughly investigate the structural parameters and phase purity Rietveld refinement was performed on experimentally XRD data. It is a method described by Hugo Reitveld used in structural analysis of the samples. The experimental XRD pattern of the synthesized sample was adopted from our previously reported work[22]. The phases of the samples were identified by matching the obtained XRD data with the standard patterns from the JCPDS database[22].The structural analysis was further refined using the Rietveld refinement method, performed with the Fullprof Suite software. For the present investigation, the simulated XRD patterns used in Rietveld analysis were generated assuming a monoclinic crystal structure belonging to the C2/c space group. The Rietveld-refined XRD plots, along with the residuals from the fitting process, are displayed for different samples in the Fig. 1(a).The crystal structure of prepared samples was drawn by VESTA software Fig.1(b). The quality of the refinement was evaluated by the chi-squared (χ^2) values, which were found to be below six for all prepared samples, indicating a reliable structural fit. Additionally, the refined parameters, including lattice parameters and various R-factors, are summarized in the Tables 1 and 2. Based on these results, it can be conclusively stated that all the samples exhibit a monoclinic crystal structure. All the observed experimental diffraction peaks were precisely assigned to their corresponding crystal planes, including the primary reflections from the (-111) and (111) Miller indices. No secondary or impurity phases were detected within the detection limits of the instrument.

The quality factors characterizing the goodness of fitting are[23-26];

Table 1 — Rietveld refined position parameters, Lattice parameters and R-factors (R_p, R_{WP}, R_{exp}), chi^2(χ^2) of samples S1, S2, and S3

Samples		Position parameters			Lattice parameters					Refined R-factors			
	Atoms	X	Y	Z	a(A^0)	b(A^0)	c(A^0)	B	V(A^0)^3	R_p	R_{WP}	R_{exp}	χ^2
S1	Cu	0.25000	0.25000	0.0000	4.7031	3.4392	5.1441	99.30	83.6829	19.9	28.0	11.63	5.81
	O	0.00000	0.32900	0.2500									
S2	Cu	0.25000	0.25000	0.0000	4.6933	3.4343	5.1451	99.24	82.9297	25.5	30.2	13.24	5.20
	O	0.00000	0.34665	0.2500									
S3	Cu	0.25000	0.25000	0.0000	4.7018	3.4351	5.1460	99.27	83.1138	22.1	28.1	12.36	5.19
	O	0.00000	0.35710	0.2500									

Table 2 — Miller indices (hkl), Bragg's angle(2θ) and interplanar spacing(d_{hkl}) from reitveld data

Samples	Planes	Multiplicity	2θ(degree)	I_{obs}	I_{cal}	d_{hkl}
S1	(110)	4	32.372	128.5	118.5	2.763306
	(-111)	4	35.430	717.9	708.0	2.531479
	(111)	4	38.531	1170.3	1154.1	2.334537
	(-202)	2	48.655	136.9	135.3	1.869819
	(020)	2	53.222	90.7	76.1	1.719647
	(202)	2	57.971	56.7	42.9	1.589551
	(-113)	4	61.379	99.4	56.9	1.509208
	(-311)	4	66.003	43.1	32.8	1.414247
	(220)	4	67.767	45.7	26.6	1.381653
S2	(110)	4	32.426	108.9	104.7	2.758826
	(-111)	4	35.488	614.0	607.5	2.527445
	(111)	4	38.576	802.8	811.0	2.331934
	(-202)	2	48.747	104.0	189.5	1.866512
	(020)	2	53.305	67.9	60.3	1.717161
	(202)	2	58.024	40.5	35.0	1.588229
	(-113)	4	61.442	79.5	47.2	1.507808
	(-311)	4	66.154	74.8	27.6	1.411381
	(220)	4	67.892	46.5	22.7	1.379413
S3	(110)	4	32.400	133.1	125.0	2.760941
	(-111)	4	35.457	733.7	729.7	2.529592
	(111)	4	38.547	891.2	896.2	2.333619
	(-202)	2	48.666	171.2	116.5	1.869426
	(020)	2	53.291	77.3	66.7	1.717588
	(202)	2	57.952	50.8	38.7	1.590021
	(-113)	4	61.382	70.9	51.8	1.509149
	(-311)	4	66.039	90.4	30.3	1.413548
	(220)	4	68.669	36.3	24.7	1.380471

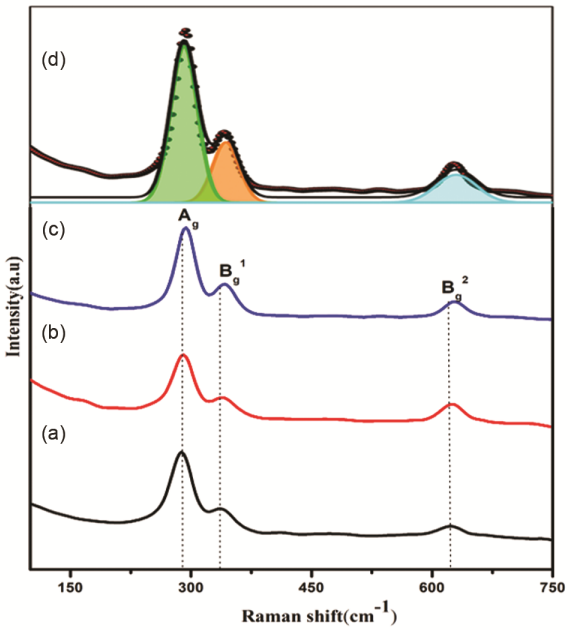


Fig. 2 — (a) Raman Spectra of prepared thin films oxidized at 400 °C, (b) 500 °C and (c) 600 °C; and (d) Deconvoluted graph of thin film S3

Weighted power factor;

$$R_{wp} = \frac{[\sum w_i(y_i(\text{obs})-y_i(\text{calc}))^2]^{\frac{1}{2}}}{\sum w_i((y_i(\text{obs}))^2} \quad \ldots (1)$$

Power factor;

$$R_p = \frac{\sum y_i\,(\text{obs})-y_i(\text{calc})}{\sum y_i\,(\text{obs})} \quad \ldots(2)$$

R Structure factor;

$$R_F = \frac{\sum\left|(I_k\,(obs))^{\frac{1}{2}}-(I_k\,(calc))^{\frac{1}{2}}\right|}{\sum(I_k\,(obs))^{\frac{1}{2}}} \quad \ldots(3)$$

R Bragg Factor;

$$R_B = \frac{\sum|(I_k\,(\text{obs})-(I_k(\text{calc}))|}{\sum I_k(\text{obs})} \quad \ldots (4)$$

where I_K represents the intensity of the K threflection. The expected R factor (R_{exp}) is defined as;

$$R_{exp} = \left[\frac{N-P}{\sum w_i(y_i\,(\text{obs}))^2}\right]^{\frac{1}{2}} \quad \ldots (5)$$

where N denotes the total number of points, P represents the number of refined parameters.

Goodness of fitting(GOF) and the chi square (χ^2) are defined as;

$$GOF = \frac{R_{wp}}{R_{exp}} \quad \ldots(6)$$

$$\chi^2 = \left(\frac{R_{wp}}{R_{exp}}\right)^2 \quad \ldots (7)$$

3.2 Vibrational Analysis

In order to confirm the nature of Cu, Raman analysis was performed for prepared films S1,S2 and

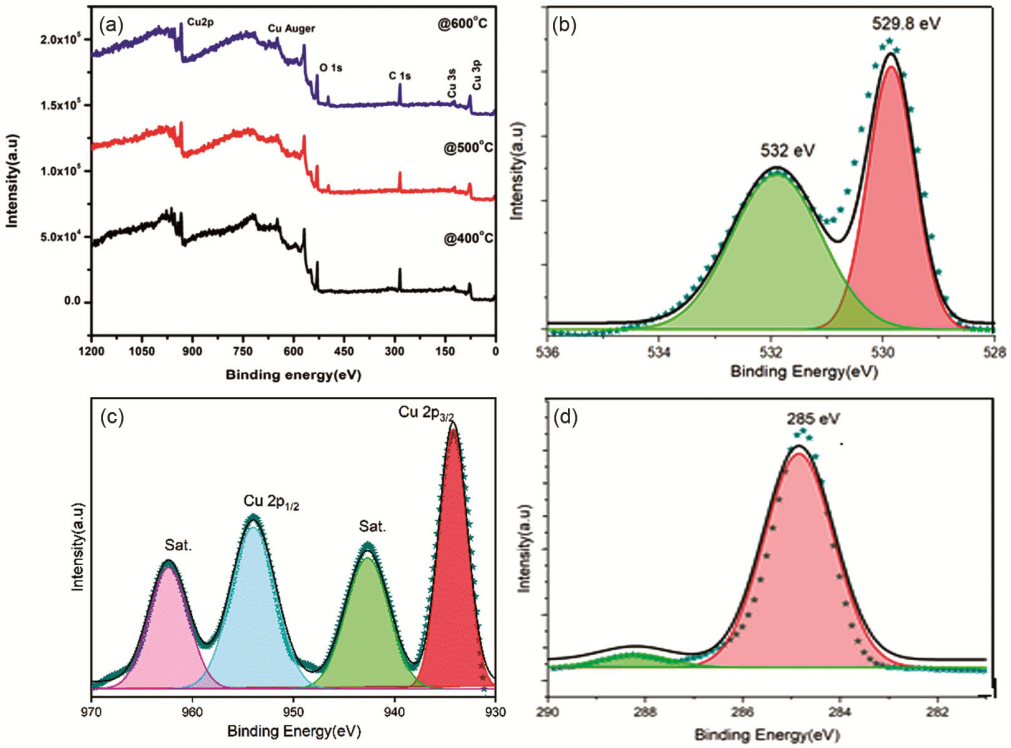


Fig. 3 — (a) XPS survey spectra of CuO thin films oxidized at 400°C, 500 °C and 600°C (b) core level O1s spectra (c) deconvoluted spectra of core level Cu2p; and (d) deconvoluted spectra of C1s

S3,shown in Fig.2(a). Figure 2(b) represents the deconvoluted spectra of S3 (film annealed at 600°C.CuO crystallizes in the C2/c monoclinic space group which was confirmed by Rietveld refinement of these prepared films and has two molecules per primitive cell. The zone-center vibrational modes for this structure contain acoustic modes (A_u+2B_u), infrared active modes (3A_u+3B_g) and Raman active modes (A_g+2B_g). The Raman spectra of all synthesized thin films (S1,S2 and S3)are identical to that reported previously for CuO because the Raman spectra confirm the presence of all three Raman active optical phonons (A_g+2B_g). In sample (c) chemical analysis show three distinct peaks at 294cm^{-1}, 343 cm^{-1}, and 630 cm^{-1} corresponding to the A_g, B_g^1, and B_g^2 phonon modes[27-29]. In Raman spectrum (b) peaks shows at 290 cm^{-1}, 342 cm^{-1}, 626 cm^{-1}, while in Raman spectrum (a) 288cm^{-1}, 238 cm^{-1}, 623 cm^{-1} these are also attributed to the A_g, B_g^1, and B_g^2 phonon modes[27,30-31]. In the Raman spectra (b) and (c), the peaks are slightly shifted to the left may be due to the difference in their synthesis temperatures. All spectrum shows high intensity peaks the presence of high purity of CuO phase.

3.3 Chemical Analysis

The chemical composition of the constituent elements was observed by, X-ray Photoelectron Spectroscopy (XPS) which was performed on the prepared films as shown in Fig. 3. Figure 3(a) shows the survey spectra of Copper oxide thin films at different temperature demonstrating the presence of copper and oxygen in the prepared films. Figure 3(b) shows the high-resolution deconvoluted XPS spectrum for sample S3, where a low intensity O1 speak observed at 532 eV with high intensity peak at 529.8 eV. The high intensity peak at 529.8 eV is located at 2.2 eV lower from the peak at 532 eV which may be due to surface oxidation. Additionally, another peak at 532 corresponds to effective oxygen in CuO, further confirming the presence of Cu^{2+} defective oxide [32-33]. Figure 3(c) shows deconvoluted spectra of Cu2p and there are two primary peaks observed at 934.7 eV (Cu 2$p_{3/2}$) and 953.8 eV (Cu 2$p_{1/2}$), accompanied by two satellite peaks at 942.7 eV and 962.3 eV demonstrating the presence of Cu^{2+} in the prepared samples. In Fig. 3(d), there is a high intensity carbon peaks at 284.8 eV demonstrating the strong C-C functional group. These findings indicate that copper ions in the films exist in

the +2oxidation state (Cu^{2+}) while confirming the complete absence of metallic phase or other phase of copper[32-36].

4 Conclusion

High quality copper oxide thin films were deposited using Electron beam evaporation technique. The crystal structure was studied using X-ray diffraction at room temperature and the Rietveld Refinement was used for detailed structural analysis. Rietveld Refinement confirmed that films have monoclinic structure with space group C2/c. Raman spectra confirmed the single phase of copper oxide which is CuO without secondary phase. XPS study revealed that Cu^{2+} oxidation state was present in prepared films which confirmed the complete transformation of copper films to copper oxide films. The combined structural and chemical analysis demonstrates that the prepared films possess improved phase purity making them suitable for applications in optoelectronics, sensing, and nonlinear optical devices.

References

1 Djebian R, Boudjema B, Kabir A & Sedrati C *Solid State Sci*, 101 (2020) 106147.
2 Parvathy T, Sabeer N M, Mohan N & Pradyumnan P P, *Optic Mater*, 125 (2022) 112031.
3 Krishna A M S, Busi K B, Ramasubramanian B, Reddy V S, Samanta A, Ramakrishna S & Dalapati G K, *Memories Mater Device Circuits Syst*, 7 (2024) 100100.
4 Naveena D, Logu T, Sethuraman K & Bose A C, *J Alloy Compound*, 795 (2019) 187.
5 Naveena D, Logu T, Dhanabal R, Sethuraman K & Bose A C, *J Mater Sci Mater Electron*, 30 (1) (2019) 561.
6 Valladares L D L S, Salinas D H, Dominguez A B, Najarro D A, Khondaker S I, Mitrelias T, & Majima Y, *Thin solid films*, 520 (20) (2012) 6368.
7 Liu A, Nie S, Liu G, Zhu H, Zhu C, Shin B & Shan F, *J Mater Chem C*, 5 (10) (2017) 2524.
8 Jilani A, Abdel-Wahab M S, Othman M H D, V K S & Alsharie A *Optik*, 144 (2017) 207.
9 Prabu R D, Valanarasu S, Kulandaisamy I, Ganesh V, Shkir M & Kathalingam A, *J Mater Sci: Mater Electron*, 28 (9) (2017) 6754.
10 Sadiq Z M, Hassan M A & Hassoon K I, *J Phys: Confer Ser*, 2322 (1) (2022) 012088.
11 Patwary M A M, Hossain M A, Ghos B C, Chakrabarty J, Haque S R, Rupa S A & Tanaka T, *RSC advances*, 12 (51) (2022) 32853.
12 Zuo J, *BN Lewis Pair-Functionalized Anthracenes: Formation of Regioisomers, Steric and Electronic Tuning, and Extension to Conjugated Polymer,* Rutgers University, (2025).
13 Diachenko O, Kováč Jr J, Dobrozhan O, Novák P, Kováč J, Skriniarova J & Opanasyuk A *Coatings*, 11 (11) (2021) 1392.
14 Xu C, Wang X, Yang L & Wu Y, *J Solid State Chem*, 182 (9) (2009) 2486.
15 Jin Z, Zhang X, Li Y, Li S & Lu G, *Catalysis Commun*, 8 (8) (2007) 1267.
16 Jilani A, Abdel-Wahab M S & Hammad A H, *Modern Technologies for creating the thin-film systems and coatings*, 2 (3) (2017) 137.
17 Rabih L, Ali G G & Younus M H, *AIP Confer Proceed*, 2201 (1) (2019) 020001.
18 Sadiq Z M, Hassan M A & Hassoon K I, *J Phys: Confer Ser*, 2322 (1) (2022) 012088.
19 Wang Y, Jiang T, Meng D, Yang J, Li Y, Ma Q & Han J, *Appl Surface Sci*, 317 (2014) 414.
20 Sadiq Z M, Hassan M A & Hassoon K I, *J Phys: Confer Ser*, 2322 (1) (2022) 012088.
21 Faisal A D & Khalef W K, *J Mater Sci: Mater Electron*, 28 (24) (2017) 18903.
22 Makkar M, Barala M, Nanda K, Gummagol N & Mohan D, *Phys Script*, 100 (6) (2025) 065958.
23 Rahman M M & Alo U K, *Int J Eng Res Sci*, 6 (2) (2020) 1.
24 Moura A P, *Adv Powder Technol*, 21 (2) (2010) 197.
25 Mandal S & Samanta P K, *Mater Today Proceed*, 60 (2022) 1051.
26 Toby B H, *Powder Diffract*, 21 (1) (2006) 67.
27 Chou M H, Liu S B, Huang C Y, Wu S Y & Cheng C L, *Appl Surface Sci*, 254 (23) (2008) 7539.
28 Maji S K, Mukherjee N, Mondal A, Adhikary B & Karmakar B, *J Solid State Chem*, 183 (8) (2010) 1900.
29 Dar M A, Ahsanulhaq Q, Kim Y S, Sohn J M, Kim W B & Shin H S, *Appl Surface Sci*, 255 (2009) 6279.
30 Rashad M, Rüsing M, Berth G, Lischka K & Pawlis A, *J Nanomater*, 1 (2013) 1.
31 Tran T H, Nguyen T M A, Dao V P T, Sai C D, Bach T C, Pham N H & Nguyen V T *Ceram Int*, 48 (3) (2022) 3199.
32 Biesinger M C, *Surface Interface Anal*, 49 (13) (2017) 1325.
33 Biesinger M C, Payne B P, Grosvenor A P, Lau L W, Gerson A R & Smart R S C, *Appl Surface Sci*, 257 (7) (2011) 2717.
34 Ungeheuer K, Bocirnea A E, Marszalek K W, Tokarz W, Pikulski D A, Kąkol Z & Galca A C, *Scientif Rep*, 15 (1) (2025) 25255.
35 Krishna A M S, Busi K B, Ramasubramanian B, Reddy V S, Samanta A, Ramakrishna S & Dalapati G K, *Mem Mater Devices Circuit Syst*, *7* (2024) 100100.
36 Dementyeva M M, Prikhodko K E, Gurovich B A, Bukina Z V, Komarov D A & Kutuzov L V, *IOP Confer Ser: Mater Sci Eng*, 256 (2017) 012020.